Am J Physiol Cell Physiol 306: C705–C713, 2014.
First published January 29, 2014; doi:10.1152/ajpcell.00390.2013.

Expression and function of a T-type Ca^{2+} conductance in interstitial cells of Cajal of the murine small intestine

Haifeng Zheng,[1]* Kyung Sik Park,[2]* Sang Don Koh,[1] and Kenton M. Sanders[1]

[1]*Department of Physiology and Cell Biology, University of Nevada, School of Medicine, Reno, Nevada; and* [2]*Department of Internal Medicine, Keimyung University School of Medicine, Daegu, Korea*

Submitted 23 December 2013; accepted in final form 24 January 2014

Zheng H, Park KS, Koh SD, Sanders KM. Expression and function of a T-type Ca^{2+} conductance in interstitial cells of Cajal of the murine small intestine. *Am J Physiol Cell Physiol* 306: C705–C713, 2014. First published January 29, 2014; doi:10.1152/ajpcell.00390.2013.—Interstitial cells of Cajal (ICC) generate slow waves in gastrointestinal (GI) muscles. Previous studies have suggested that slow wave generation and propagation depends on a voltage-dependent Ca^{2+} entry mechanism with the signature of a T-type Ca^{2+} conductance. We studied voltage-dependent inward currents in isolated ICC. ICC displayed two phases of inward current upon depolarization: a low voltage-activated inward current and a high voltage-activated current. The latter was of smaller current density and blocked by nicardipine. Ni^{2+} (30 μM) or mibefradil (1 μM) blocked the low voltage-activated current. Replacement of extracellular Ca^{2+} with Ba^{2+} did not affect the current, suggesting that either charge carrier was equally permeable. Half-activation and half-inactivation occurred at −36 and −59 mV, respectively. Temperature sensitivity of the Ca^{2+} current was also characterized. Increasing temperature (20–30°C) augmented peak current from −7 to −19 pA and decreased the activation time from 20.6 to 7.5 ms [temperature coefficient (Q_{10}) = 3.0]. Molecular studies showed expression of *Cacna1g* (Cav3.1) and *Cacna1h* (Cav3.2) in ICC. The temperature dependence of slow waves in intact jejunal muscles of wild-type and *Cacna1h*$^{-/-}$ mice was tested. Reducing temperature decreased the upstroke velocity significantly. Upstroke velocity was also reduced in muscles of *Cacna1h*$^{-/-}$ mice, and Ni^{2+} or reduced temperature had little effect on these muscles. Our data show that a T-type conductance is expressed and functional in ICC. With previous studies our data suggest that T-type current is required for entrainment of pacemaker activity within ICC and for active propagation of slow waves in ICC networks.

gastrointestinal smooth muscle; pacemaker; slow wave; gastrointestinal motility

COORDINATION OF CONTRACTIONS, in some cases over many centimeters of bowel wall, requires regulatory mechanisms beyond the spontaneous excitability of smooth muscle cells (SMCs). For example, rhythmic electrical depolarizations, known as slow waves, time the phasic contractions of segmentation and peristalsis in the small intestine (21, 32). Interstitial cells of Cajal (ICC) are the cells that generate pacemaker activity and propagate slow waves actively in gastrointestinal muscles (4, 11, 19, 25, 28, 33, 36). Slow waves conduct to SMCs via gap junctions, but SMCs lack the ionic mechanisms necessary for active propagation of slow waves (30). Depolarization of SMCs caused by slow waves leads to enhanced open probability of voltage-dependent, dihydropyridine-sensitive Ca^{2+} channels, and the resulting influx of Ca^{2+} induces excitation-contraction coupling (26).

Slow waves result from activation of a large inward current (aka slow wave current) carried by Cl^- ions (9, 39). The basic pacemaker event is release of Ca^{2+} from intracellular stores and localized activation of Cl^- channels, encoded by *Ano1* (12, 39). These events are stochastic in nature and referred to as spontaneous transient inward currents (STICs; see Refs. 10, 40). Cells in situ, in the absence of voltage control, depolarize in response to STICs producing spontaneous transient depolarization events [STDs; also termed "unitary potentials" by Hirst and Edwards (10)]. A voltage-dependent mechanism appears to entrain STICs into whole cell slow wave currents, and this is why step depolarization can activate (or pace) slow waves (7, 39). A similar mechanism is likely to be responsible for cell-to-cell active propagation of slow waves.

Most investigators agree that propagation of slow waves through networks of ICC depends on a voltage-dependent mechanism (5, 15, 34), but the precise mechanism has been controversial. It is clear that propagation depends on gap junction coupling between cells because β-glycyrrhetinic acid, which does not block pacemaker activity in individual cells, blocks the ability of slow waves to spread cell-to-cell coherently (27). It also appears that the voltage-dependent step includes, or is reinforced by, release of Ca^{2+} from inositol triphosphate (IP_3) receptor-operated stores because 2-aminoethoxydiphenyl borate and xestospongin C block slow waves and propagation (8, 21, 27, 35). Some investigators have suggested that depolarization activates phospholipase C and causes generation of IP_3, release of Ca^{2+}, and activation of Ca^{2+}-activated Cl^- current (24). However, there is also evidence suggesting that depolarization activates a Ca^{2+} conductance, and Ca^{2+} entry could couple to release from stores via Ca^{2+}-induced Ca^{2+} release (1, 17, 18). Pharmacological evidence provided in these studies suggests that a T-type conductance may be responsible for voltage-dependent Ca^{2+} entry because T channel blockers inhibited slow wave propagation. A study of cultured cells reported the presence of a T-type current in ICC (15); however, concerns about this finding have been raised since ion channel expression changes in culture (39). In the present study we have examined the expression of voltage-dependent inward currents in freshly dispersed ICC from the murine small intestine that were identified unequivocally by constitutive expression of a fluorescent reporter.

MATERIALS AND METHODS

Tissue preparation. C57BL/6 (Jackson Laboratory, Bar Harbor, ME), smMHC/Cre/eGFP (donated by Michael Kotlikoff, Cornell University), Cacna1h$^{-/-}$ mice (donated by Dr. Kevin P. Campbell, University of Iowa), and Kit$^{copGFP/+}$ mice were used for these

* H. Zheng and K. S. Park contributed equally to this work.

Address for reprint requests and other correspondence: K. M. Sanders, Dept. of Physiology and Cell Biology, Univ. of Nevada, School of Medicine, Reno, NV 89557 (e-mail: ksanders@medicine.nevada.edu).

experiments. Animals were anaesthetized with isoflurane (Aerrane; Baxter, Deerfield, IL) before decapitation and then small intestines were removed. The Institutional Animal Use and Care Committee at the University of Nevada approved all procedures used in the breeding and killing of animals.

Isolation of cells. ICC and SMCs were isolated from $Kit^{+/copGFP}$ mice described previously (39) and smMHC/Cre/eGFP mice, respectively. Small strips of jejunal muscle were dissected and equilibrated in Ca^{2+}-free Hanks' solution for 20 min. Cells were dispersed from these strips, with an enzyme solution containing the following (per ml): collagenase (1.3 mg. Worthington Type II), bovine serum albumin (2 mg; Sigma, St. Louis, MO), trypsin inhibitor (2 mg; Sigma) and ATP (0.27 mg). Cells were plated onto sterile glass coverslips coated with murine collagen (2.5 mg/ml; BD Falcon, Franklin Lakes, NJ) in 35-mm culture dishes. Freshly dispersed $copGFP^+$ cells were allowed to stabilize for 3 to 6 h at 37°C in an incubator (atmosphere 95% O_2-5% CO_2) in smooth muscle growth medium (Clonetics, San Diego, CA) supplemented with 2% antibiotic-antimycotic (GIBCO, Grand Island, NY) and stem cell factor (5 ng/ml; Sigma).

Electrophysiological recording. ICC were identified as cells with green fluorescent protein using an inverted fluorescence microscope. The standard whole cell patch clamp configuration was employed to record membrane currents (voltage clamp). Currents were amplified with an Axopatch 200B patch-clamp amplifier (Axon Instruments, Union City, CA) and digitized with a 16-bit analog to digital converter (Digidata 1440A; Axon Instruments) and stored directly online using pCLAMP software (version 10.2; Axon Instruments). Data were sampled at 4 kHz and filtered at 2 kHz using an eight-pole Bessel filter for whole cell experiments. All data were analyzed using clampfit (pCLAMP version, 10.2; Axon Instruments) and Graphpad Prism (version 3.0; Graphpad Software, San Diego, CA) software. Average capacitance of freshly dispersed ICC was 5.2 ± 0.6 pF. External solution for whole cell recordings was a Ca^{2+}-containing physiological salt solution (CaPSS) containing the following (in mM): 5 KCl, 135 NaCl, 2 $CaCl_2$, 10 glucose, 1.2 $MgCl_2$, and 10 HEPES adjusted to pH 7.4 with Tris. The pipette solutions contained the following (in mM): 120 CsCl, 20 TEACl, 10 BAPTA, 10 HEPES, 2 MgATP, and 0.1 NaGTP, pH adjusted to 7.2 by Tris.

For the measurement of intracellular membrane potentials, jejunal muscles from C57BL/6 and *Cacna1h*$^{-/-}$ mice were prepared by removing the mucosa. Muscle strips (10 × 5 mm) were pinned to Sygard (Dow Corning, Midland, MI) floor of a recording chamber with circular muscle facing upward. The bath chamber was perfused with Krebs-Ringer buffer (KRB) containing the following (in mM): 120 NaCl, 5.9 KCl, 1.2 $MgCl_2$, 15.5 $NaHCO_3$, 1.2 NaH_2PO_4, 11.5 dextrose, and 2.5 $CaCl_2$ pH 7.4 adjusted by bubbling with 95% O_2−5% CO_2 at 37°C. Circular muscle cells were impaled with glass microelectrodes (50−80 MΩ) filled with 3 M KCl. Membrane potentials were measured with a high impedance electrometor (Duo-773; WPI, Sarasota, FL) and digitized using an analog to digital converter (Digidata 1322A; Axon Instruments). All data were analyzed using pCLAMP 10.2 (Clampfit; Axon Instruments) and Graphpad Prism 3.0 (Graphpad Software, San Diego, CA).

Cell collecting and PCR. $copGFP^+$ ICCs and eGFP-SMCs were purified by fluorescence-activated cell sorting (FACS; Becton-Dickinson FACSAria) using 488-nm excitation and a 530/30-nm bandpass filter for green fluorescent protein. Total RNA was isolated from $copGFP^+$ ICC, eGFP-SMCs, and unsorted cells using illustra RNAspin Mini RNA isolation kit (GE Healthcare, Little Chalfont, UK), and first-strand cDNA was synthesized using SuperScript III (Invitrogen, Carlsbad, CA), according to the manufacturer's instructions. PCR was performed with specific primers using AmpliTaq Gold PCR Master Mix (Applied Biosystems, Foster City, CA). Primer sequences are shown in Table 1. PCR products were analyzed on 2% agarose gels and visualized by ethidium bromide. Quantitative PCR (qPCR) was performed with the same primers used for PCR using Syber green chemistry on the 7300 Real Time PCR System (Applied Biosystems). Regression analysis of the mean values of eight multiplex qPCRs for the log10 diluted cDNA was used to generate standard curves. Unknown amounts of messenger RNA (mRNA) were plotted relative to the standard curve for each set of primers and graphically plotted using Microsoft Excel. This gave transcriptional quantification of each gene relative to the endogenous hypoxanthine guanine phosphoribosyltransferase (*Hprt*) standard after log transformation of the corresponding raw data.

Statistical analyses. Data are expressed as means ± SE of *n* cells. All statistical analyses were performed using Graphpad Prism. We used Student's *t*-test to compare single values under control and experimental conditions or ANOVA with Dunnett's post-hoc analysis to compare groups of data. In all statistical analyses, $P < 0.05$ was considered statistically significant.

Table 1. *Primer sequences*

Gene Name/Primer Sequence	Product Length, bp	Accession Number
Hprt		
F-GACTTGCTCGAGATGTCATGAAGGAGAT	198	NM_013556
R-TGTCCCCCGTTGACTGATCATTACAGTA	(Exons 3–4)	
Cacna1g		
F-ACA ACG GCA TGG CCT CCA CGT	137	NM_009783
R-CCG TTT GCC GAT TTC CTC TGC CTG	(Exons 13–14)	
Cacna1h		
F-TGG AGA CCT ACA CAG GCC CGG T	149	NM_021415
R-CAG AGA GCG GGG CGT ATC CC	(Exons 40–41)	
Cacna1i		
F-ACC AAC CCT GAC GTC CCG CA	120	NM_001044308
R-CAC ACA CTC GAA CCA CGG GTT ACA	(Exons 3–4)	
Myh11		
F-CAGCTGGAAGAGGCAGAGGAGG	198	NM_013607
R-AACAAATGAAGCCTCGTTTCCTCTC	(Exons 40–41)	
cKit		
F-CGCCTGCCGAAATGTATGACG	162	NM_021099
R-GGTTCTCTGGGTTGGGGTTGC	(Exons 19–20)	
Pdgfra		
F-ATGACAGCAGGCAGGGCTTCAACG	195	NM_011058
R-CGGCACAGGTCACCACGATCGTTT	(Exons 5–6)	

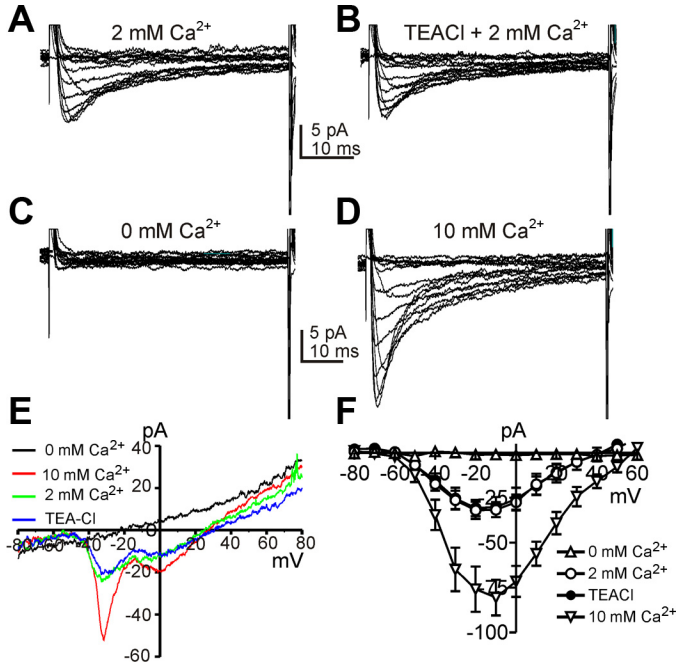

Fig. 1. Two types of voltage-dependent Ca^{2+} currents in interstitial cells of Cajal (ICC). *A–D*: representative traces recorded in 2 mM Ca^{2+}, 0 mM Na^{+} (TEA), 0 mM Ca^{2+}, and 10 mM Ca^{2+}, respectively. Data were obtained by steps from −80 to 60 mV every 10 s with 10-mV increments. *E*: cells were also depolarized from −80 to 80 mV by ramp protocols. The inward current was sensitive to extracellular Ca^{2+}. *F*: current-voltage (*I–V*) relationships for the inward current (means ± SE) from 5 cells using step protocols to more accurately determine reversal potentials in 0 mM Ca^{2+} (△), 2 mM Ca^{2+} (○), 0 mM Na^{+} (TEA; ●), and 10 mM Ca^{2+} (▽). The pattern of the *I–V* relationships is different using ramp protocols (*E*) and step protocols (*F*) due to the inactivation properties of the Ca^{2+} conductances.

RESULTS

Characterization of two types of inward currents in ICC. For characterization of voltage-dependent inward currents, a Cs^{+}-rich pipette solution with a high concentration of BAPTA (10 mM, see MATERIALS AND METHODS) was used to minimize contamination from the large amplitude of Ca^{2+}-activated Cl^{-} currents expressed by these cells (39). We tested the effects of varying external Ca^{2+} ($[Ca^{2+}]_o$) from 0 to 10 mM. The cells were held at −80 mV and stepped from −80 to +60 mV in 10-mV increments. Figure 1, *A–D*, shows representative current responses to step depolarizations in the presence of different $[Ca^{2+}]_o$. After each solution change, a voltage ramp protocol (from −80 to +80 mV for 400 ms) was applied to show the effects of each solution on the current-voltage (*I–V*) relationship (Fig. 1*E*). When cells were exposed to 2 mM $[Ca^{2+}]_o$, two types of voltage gated inward currents were recorded (Fig. 1, *A* and *E*). One conductance (low voltage-activated inward current) activated and reached a peak at between −30 and −20 mV (−6.0 ± 0.2 pA/pF; $n = 5$) and the second conductance (high-voltage activated inward current) activated and reached peak at 0 mV (−5.5 ± 0.7 pA/pF; $n = 5$; Fig. 1*E*). Equimolar replacement of extracellular Na^{+} with TEA to test the contribution of a Na^{+} conductance did not affect the inward current responses (Fig. 1, *B* and *E*). When $[Ca^{2+}]_o$ was reduced to a nominally Ca^{2+}-free solution (0 mM), both phases of the inward current response was abolished (Fig. 1, *C* and *E*). The reversal potential for the whole cell current shifted dramatically to negative potentials under these circumstances (Fig. 1*E*). Increasing $[Ca^{2+}]_o$ from 2 to 10 mM increased both types of inward currents (e.g., from −33.0 ± 5.1 to −87.8 ± 5.0 pA at −20 mV and from 30.3 ± 5.5 to −77.4 ± 8.0 pA at 0 mV; $n = 5$) and shifted the reversal potential from +41.9 ± 0.6 to +57.5 ± 0.4 mV ($n = 5$; Fig. 1, *D* and *F*). These data show that the voltage-dependent inward currents in ICC are both due to Ca^{2+} conductances. Current-voltage relationships obtained from step protocols performed on 5 cells are summarized in Fig. 1*F*. These data indicate that both the inward currents are Ca^{2+}-permeable and low voltage-activated inward currents are highly expressed in ICC.

L-type Ca^{2+} channels have been shown to be more permeable to Ba^{2+} than to Ca^{2+}, and T-type Ca^{2+} channels are equally permeable to Ca^{2+} and Ba^{2+} (3). We examined inward current responses after extracellular Ba^{2+} ($[Ba^{2+}]_o$) replacement of $[Ca^{2+}]_o$. In these experiments we first tested the effects of increasing $[Ca^{2+}]_o$ from 2 to 10 mM (Fig. 2, *B* and *C*). Elevated $[Ca^{2+}]_o$ increased both components of inward current. Replacement of $[Ca^{2+}]_o$ (10 mM) with $[Ba^{2+}]_o$ (10 mM) increased the high voltage-activated inward current by 76 ± 16% at 0 mV but did not enhance the low voltage-activated inward current (Fig. 2, *A–C*; $n = 5$). These data suggest that ICC express both L-type and T-type Ca^{2+} conductances.

We also examined the pharmacological profiles of the Ca^{2+} conductances in ICC by testing drugs and ions traditionally described as T-type and L-type Ca^{2+} channel blockers. The same step depolarization and ramp (400 ms) protocols described in Fig. 1 were utilized in these experiments. Nicardipine (1 μM, L-type Ca^{2+} channel blocker) completely blocked

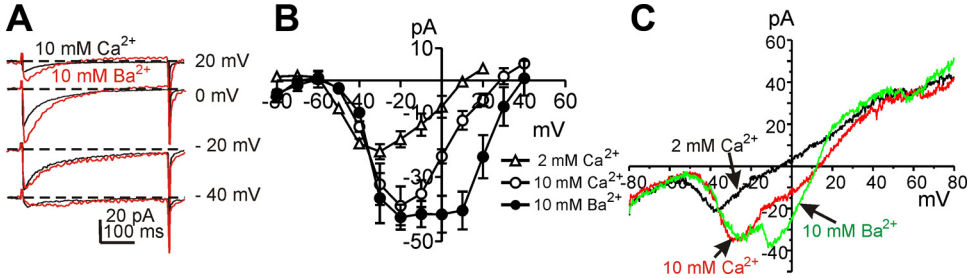

Fig. 2. Ba^{2+} permeability of two types of inward currents in ICC. *A*. Representative current traces recorded with 10 mM Ca^{2+} or 10 mM Ba^{2+}, respectively. Steps were applied to −40,−20, 0, and 20 mV from a holding of −80 mV in 10 mM Ca^{2+} (black lines) or 10 mM Ba^{2+} (red lines). *B*. current-voltage relationships for peak current (means ± SE) in 2 mM Ca^{2+} (△), 10 mM Ca^{2+} (○), and 10 mM Ba^{2+} (●). *C*: currents were obtained by ramp depolarization from −80 to +80 mV in 2 mM Ca^{2+}, 10 mM Ca^{2+}, and 10 mM Ba^{2+}.

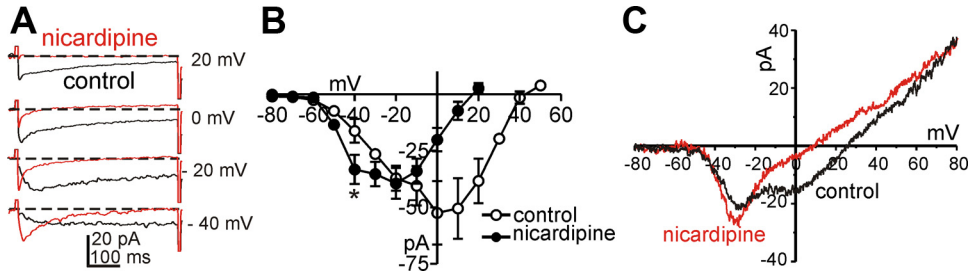

Fig. 3. Effects of nicardipine on Ca^{2+} currents in ICC. *A*: Ca^{2+} currents were recorded by voltage steps at −40, −20, 0, and 20 mV in control (black line) and nicardipine (1 μM, red line) presence. *B*: current-voltage relationships for peak current in control (○) and nicardipine (●). Nicardipine blocked high voltage-activated Ca^{2+} currents. *C*: currents traces recorded by ramp pulses from −80 to +80 mV in control (black line) and the presence of nicardipine (1 μM, red line).

the high voltage-activated currents, but the low voltage-activated current was not blocked, and in fact, the magnitude of the low voltage-activated current increased significantly in the presence of nicardipine (Fig. 3, *A* and *B*). Similar results were observed during ramp depolarization (Fig. 3*C*). Threshold potentials for resolvable low voltage-activated currents were around −60 mV (Fig. 3*B*). Current density at −20 mV was 6.6 ± 1.3 pA/pF in the presence of nicardipine, and nicardipine-sensitive current densities at 0 mV was 5.0 ± 1.3 pA/pF. Thus the T-type and L-type current density were not different in ICC ($P = 0.4$; $n = 5$). Summarized data are shown in Fig. 3*B* ($n = 5$). We further tested the effects of T-type Ca^{2+} channel blockers on the nicardipine-resistant currents. Ni^{2+} (30 μM, T-type channel blocker) completely abolished the low-voltage activated current (Fig. 4, *A* and *B*). Summarized data are shown in Fig. 4*C* ($n = 5$). Mibefradil (1 μM), another T-type channel blocker, had the same effect as Ni^{2+} on the low voltage-activated current (Fig. 4, *D* and *F*; $n = 5$). Taken together, these data suggest expression of L-type and T-type Ca^{2+} conductances in ICC. Because of the importance of T-type conductances in slow waves in intact muscles (37), we concentrated the remainder of the study on this component of inward current.

Voltage and temperature dependence of T-type Ca^{2+} channel in ICC. Further experiments to examine the voltage dependence of the T-type Ca^{2+} conductance in ICC were performed in the presence of nicardipine (1 μM; Fig. 5*A*). A double-pulse protocol was used to characterize the steady-state inactivation of the T-type conductance. Prepulse potentials (150 ms) ranging from −80 to +60 mV in 5-mV increments were applied. Following a 1-ms interpulse step to −80 mV, membrane potential was stepped to a test potential of −30 mV for 90 ms. The currents resulting from the test depolarization were normalized to the current obtained at −80 mV (I/I_{max}) and plotted against the prepulse potentials. Plotted data were fitted by a Boltzmann equation. The half-inactivation voltage was −59.2 ± 0.4 mV with a mean slope of 4.9 ± 0.4 mV (Fig. 5*B*; $n = 5$). To evaluate steady-state activation relationships, the peak conductance at each test potential was calculated using the equation: $I_{Ca} = g_{Ca} \times (V - E_{rev})$, where g_{Ca}, V, and E_{rev} are peak conductance, test potential, and reversal potential, respectively. Steady-state activation curves were constructed by normalization of the maximum conductance (G/G_{max}). The voltage of half-activation was −35.7 ± 3.2 mV with a mean slope of 12.1 ± 3.7 mV (Fig. 5*B*; $n = 5$).

Next, we tested the temperature sensitivity of the T-type Ca^{2+} conductance, because this is an important property of T-type Ca^{2+} channels (13). Step depolarizations were applied repetitively from a holding potential of −80 to −30 mV (Fig. 6*A*). Increasing temperature from 20°C to 30°C increased the amplitude of the T-type Ca^{2+} currents from −7.0 ± 1.9 to −19.5 ± 3.8 pA (Fig. 6*B*; $n = 5$; $P = 0.004$; $F = 17.84$ by ANOVA) and decreased the activation time constant from 19.0 ± 1.9 to 7.5 ± 0.1 ms (Fig. 6*C*; $n = 5$; $P = 0.001$; $F = 15.09$ by ANOVA). The temperature coefficient (Q_{10}) for amplitude was 2.8 and for the rate of activation time constant was 2.5.

Molecular candidate for T-type Ca^{2+} channels in ICC and its functional role on slow waves. Transcriptional expression of *Cacna1g* ($Ca_V3.1$), *Cacna1h* ($Ca_V3.2$), and *Cacna1i* ($Ca_V3.3$) subunits of T-type Ca^{2+} channel were tested by RT-PCR on extracts of ICC and SMC purified by FACS (see Methods).

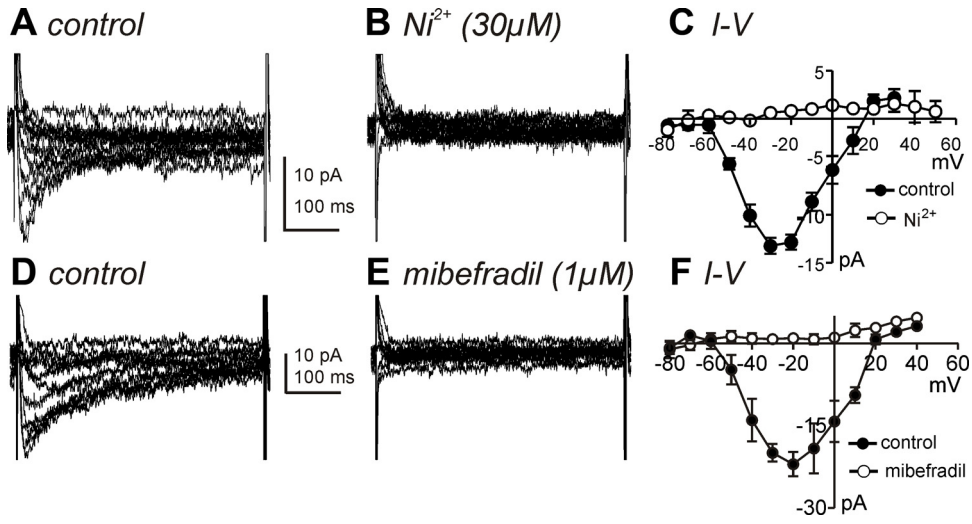

Fig. 4. Effects of T-type Ca^{2+} channel blockers on low voltage-activated Ca^{2+} currents of ICC in the presence of nicardipine. *A* and *B*: T-type Ca^{2+} currents were recorded by voltage steps from −80 to +50 mV in control and Ni^{2+} (30 μM) in the presence of nicardipine (1 μM). *C*: *I–V* relationships for peak current in control (●) and Ni^{2+} (○). Ni^{2+} completely blocked low voltage-activated Ca^{2+} currents. *D* and *E*: T-type Ca^{2+} currents were recorded by voltage steps from −80 to +60 mV in control and mibefradil (1 μM) in the presence of nicardipine (1 μM). *F*: *I–V* relationships for peak current in control (●) and mibefradil (○). Mibefradil completely blocked low voltage-activated Ca^{2+} currents.

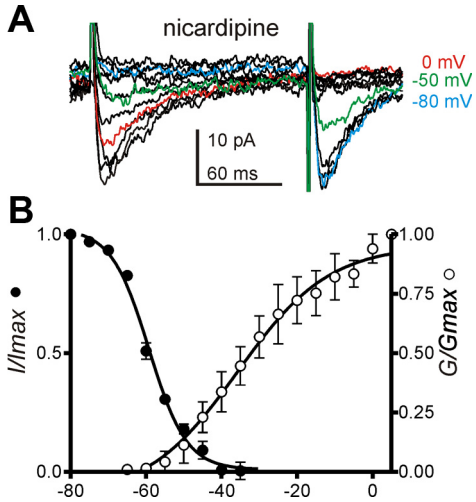

Fig. 5. Voltage dependence of activation and inactivation of T-type Ca^{2+} channel in ICC. *A*: representative traces of current evoked by applying a prepulse from −80 to 60 mV with 5-mV increments following by currents evoked at −30 mV from a brief holding potential of −80 mV in the presence of nicardipine. Blue, green, and red lines denote the traces elicited using prepotentials at −80, −50, and 0 mV, respectively. *B*: voltage dependence of steady-state activation (G/G_{max}) and inactivation (I/I_{max}) was fit with Boltzmann equation.

Primers are provided in Table 1. *Cacna1h* (Cav3.2) was expressed in SMC and ICC; however, *Cacna1g* (Cav3.1) was resolved only in extracts of ICC (Fig. 7*A*). *Kit* mRNA was amplified in sorted ICC, and *Myh11* was amplified in sorted SMCs vs. unsorted cells, confirming the relative purity of the sorted cells. Quantitative PCR showed *Cacna1h* is highly expressed in ICC and SMC. *Cacna1g* is also expressed in ICC but at a lower level compared with *Cacna1h*. There was negligible expression of *Cacna1i* in either ICC or SMC (Fig. 7*B*).

Role of T-type Ca^{2+} channel in slow waves in situ. Ni^{2+} and mibefradil were shown to reduce the slope of the upstroke phase of slow waves from small intestinal ICC of wild-type mice previously (18). In this study we tested the role of T-type Ca^{2+} channels in slow waves by testing the effects of temperature on slow waves in jejunal smooth muscles in wild-type and *Cacna1h*$^{-/-}$ mouse. The frequency of slow waves in *Cacna1h*$^{-/-}$ mice decreased significantly compared with wild-type mice as previously reported (6). Reducing temperature decreased the upstroke velocity of slow waves significantly from 0.24 ± 0.05 at 37 to 0.07 ± 0.01 at 31°C in wild type (Q_{10} = 8.7; n = 6; Fig. 8*A*). Q_{10} was determined by the changes in the maximum slope. Ni^{2+} (30 μM) also decreased the maximum slope of the upstroke phase of slow waves. In the presence of Ni^{2+} (30 μM), changing temperature had little effect on the slow wave upstroke slope (Fig. 8*B*). Figure 8*C* shows the average change in maximum slope before and after Ni^{2+} following temperature changes applied to muscles of five animals. Ni^{2+} significantly decreased the temperature sensitivity on the rate of rise of slow waves (Q_{10} = 1.4). Slow waves recorded from jejunal muscles of *Cacna1h*$^{-/-}$ mice were not decreased significantly by reduced temperature (Fig. 8, *D* and *F*) or Ni^{2+} (Fig. 8*E*; n = 4). These data suggested that Cav3.2 is a major conductance generating the slow wave upstroke in the small intestine.

DISCUSSION

It has been proposed that voltage-dependent Ca^{2+} entry, possibly via a T-type conductance, is responsible for entrainment and propagation of pacemaker currents in ICC (1, 30). In this study we showed that ICC, freshly isolated from the murine small intestine, expresses voltage-dependent Ca^{2+} currents. Two components of voltage-dependent Ca^{2+} conductance, a low voltage-activated Ca^{2+} current and a high voltage-activated Ca^{2+} current, were distinguished in whole cell patch-clamp recordings. Since slow waves in intact muscles are not typically blocked by dihydropyridines, it is unlikely that the high voltage-activated conductance is of prime importance. Therefore, we concentrated our experiments on the properties and pharmacology of the low voltage-activated conductance and concluded that it results from T-type Ca^{2+} channels, most probably encoded by *Cacna1h* and *Cacna1g*. Electrophysiological evidence supported the idea that the low-voltage activated Ca^{2+} current was due to T-type conductance, because the currents were as follows: *1*) activated and inactivated at potentials (i.e., half activation = −36 mV and half inactivation = −59 mV) consistent with the properties of expressed *Cacna1h* channels (13); *2*) blocked by Ni^{2+} and mibefradil; *3*) not blocked by nicardipine; *4*) the same magnitude when charge was carried by Ba^{2+} or Ca^{2+} (implying equal permeable); and *5*) temperature sensitive and consistent with properties of expressed *Cacna1h* channels (13). Many of the properties and pharmacology that would be consistent with the involvement of a T-like conductance have been demonstrated, as discussed below, in experiments on muscles from several regions of the gastrointestinal tract and from several species previously. The temperature dependence of slow waves in wild-type muscles and the absence of this property in muscles lacking *Cacna1h* were demonstrated in the current study. Our molecular data also showed a low level of expression of *Cacna1g*; however, both Ni^{2+} and temperature sensitivity were absent in *Cacna1h*$^{-/-}$ mice suggesting that *Cacna1h* is the dominant species of T-type Ca^{2+} channels in murine jejunum. Thus our data document a conductance that is likely to be involved in organizing local-

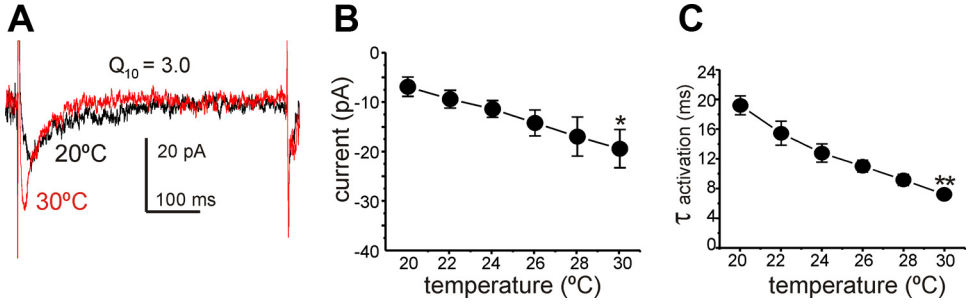

Fig. 6. Temperature sensitivity of T-type Ca^{2+} currents in ICC. *A*: representative traces of current recorded by applying a pulse from −80 to −30 mV in 20°C (black trace) and 30°C (red trace). *B*: summary of peak current at various temperature (from 20 to 30°C; n = 5). *C*: summary of activation time constant at various temperatures (n = 5) *P < 0.05, **P < 0.01 vs. 20°C.

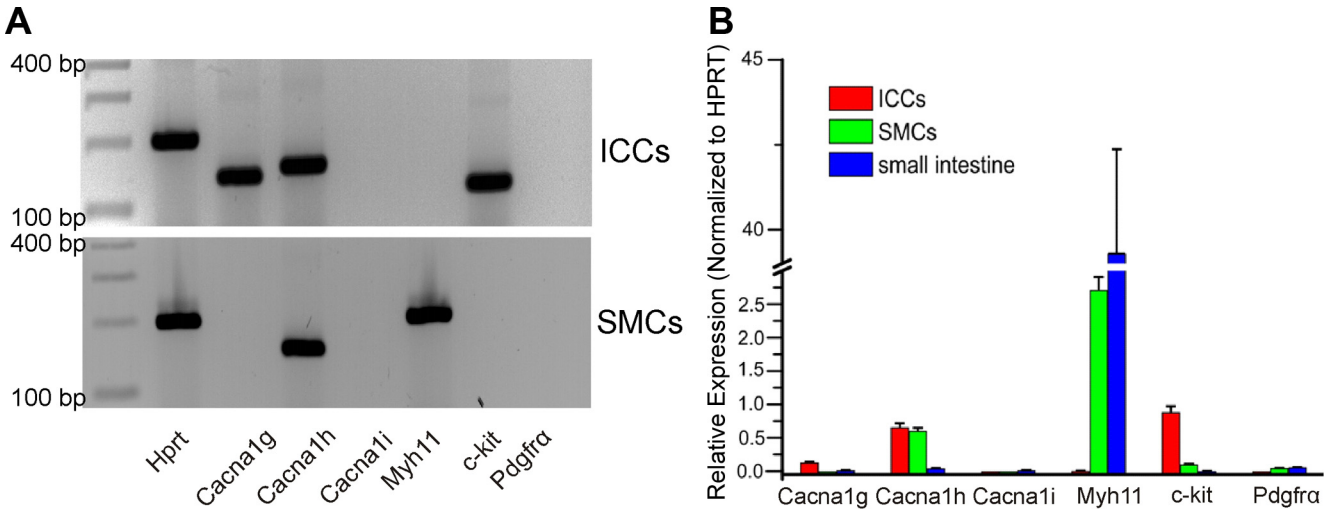

Fig. 7. Qualitative and quantitative PCR of T type calcium channels in sorted ICC, smooth muscle cells (SMCs), and unsorted (whole small intestine smooth muscle). *A*: sorted ICC displayed no contamination of SMC or PDGFRα^+ cells. *Top*: Cacna1g and Cacna1h transcripts were detected in sorted ICC. *Bottom*: Cacna1h detection in sorted SMC. *B*: quantitative analysis of PCR products demonstrated that Kit was highly enriched in ICC. Cacna1h was dominantly expressed in ICC and SMCs compared with whole small intestine. Relative expressions of all transcripts were normalized to *Hprt*.

ized STICs in ICC into whole cell slow wave currents and providing a voltage-dependent mechanism for cell-to-cell propagation of slow waves in ICC networks.

Slow waves recorded directly from ICC in the murine small intestine were greatly reduced in frequency, amplitude, and upstroke velocity by Ni^{2+} and mibefradil, as shown previously (17, 18). Slow waves were also reduced in frequency, amplitude, and upstroke velocity by reducing $[Ca^{2+}]_o$ to nominally Ca^{2+} free conditions or by elevated (20 mM) $[K^+]_o$, which depolarized ICC to −40 mV (17). The effects of high $[K^+]_o$ might be explained by the inactivation of the low voltage-activated conductance we observed in ICC, because at −40 mV the conductance was <10% available for activation. Propagation of slow waves in intact muscles is also strongly dependent on a Ca^{2+} entry mechanism that appears to be consistent with a T-type Ca^{2+} conductance. Nifedipine had no effect on slow wave propagation rate or upstroke velocity, but Ni^{2+} progressively decreased these parameters and blocked propagation at 100 μM (1). The effects of mibefradil and reduced $[Ca^{2+}]_o$ were similar, with total block of slow wave propagation at 25 and 0.5 μM, respectively. Depolarization with 15 mM $[K^+]_o$ also blocked propagation. The current study demonstrates a conductance in ICC that can explain previous observations and suggests that a T-type conductance is a fundamental component of the apparatus in ICC required for pacemaker activity.

Some investigators have suggested that the voltage sensor in ICC responsible for propagation is voltage-dependent enhancement of phospholipase C activity and/or voltage-dependent "sensitization" of IP_3 receptors (5, 14, 24). Increasing IP_3 synthesis or increasing the sensitivity of IP_3 receptors might facilitate synchronization of Ca^{2+} release in ICC and serve to entrain STICs into slow wave currents. In fact based on the properties of IP_3 receptors, increasing either IP_3 or $[Ca^{2+}]_i$ would tend to enhance the probability of Ca^{2+} release, so either mechanism might be considered an effective means of "sensitizing" IP_3 receptors (20). Although voltage-dependent regulation of IP_3 receptor-operated Ca^{2+} release has been

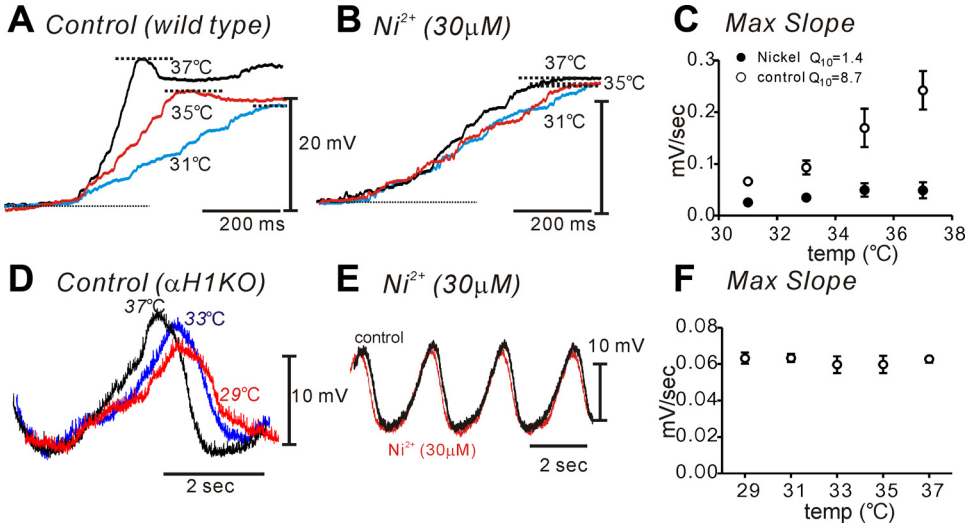

Fig. 8. Role of T-type Ca^{2+} currents on initial upstroke of slow waves in murine jejunal smooth muscle from wild-type and *Cacna1h*$^{-/-}$ mice. *A*: raising temperature from 31 to 37°C increased the initial upstroke slope of slow wave in wild-type jejunum. *B*: pretreatment of Ni^{2+} (30 μM) abolished temperature sensitivity of the initial slope in wild-type jejunum. *C*.: summarized data of maximum slope of initial upstroke before (○) and after Ni^{2+} (●) at various temperatures in wild-type jejunum. *D*: *Cacna1h*$^{-/-}$ mouse did not show the temperature sensitivity. *E*: Ni^{2+} treatment also did not show significant changes of initial upstroke slope and frequency of slow waves in *Cacna1h*$^{-/-}$. *F*: summarized data of maximum slope of initial upstroke in Cacna1h$^{-/-}$ jejunum.

demonstrated in megakaryocytes (22), such a mechanism has not been observed directly in ICC. Testing this hypothesis will require monitoring subcellular Ca^{2+} responses to agonists or IP_3 under voltage-clamp conditions, and these experiments have not yet been accomplished in isolated ICC. Therefore, at present we cannot exclude the possibility that a voltage sensor linked to IP_3 production and/or receptor affinity is involved in slow wave propagation, but results to date strongly support the importance of voltage-dependent Ca^{2+} entry through a T-type conductance in both entrainment of localized pacemaker events (STICs) into whole cell slow wave currents and in cell-to-cell slow wave propagation.

The slopes of the upstroke depolarizations of slow waves of guinea-pig antrum and murine small intestine are sensitive to changes in temperature (16, 23). Higher temperatures increase upstroke velocity and overall frequency without changing resting membrane potentials. The temperature dependence of the upstroke depolarization may be another indication of the role of T-type currents in initiation of slow waves. In the present study lowering temperature decreased the slope of the upstroke depolarization significantly. The temperature sensitivity of the upstroke was abolished by pretreatment with Ni^{2+}. Thus, based on the significant temperature sensitivity of T-type Ca^{2+} currents in ICC, it is possible that these channels contribute to slow wave upstrokes. Our molecular data suggest that *Cacna1h* is the dominant T-type Ca^{2+} channel expressed in ICC. Therefore, we also examined slow wave activity and slopes of upstroke potentials in jejunal muscles from *Cacna1h*$^{-/-}$ mice. The upstroke depolarizations of slow waves in these muscles lacked significant temperature dependence and responses to Ni^{2+}. These results are consistent with a role for channels encoded by *Cacna1h* in the initial depolarization phase of slow waves.

This study provides direct measurement of another critical element of the pacemaker mechanism driving slow wave activity in ICC. Previous studies showed voltage-dependent activation of inward currents in freshly isolated ICC from murine small intestine (7, 39), and this conductance was later shown to be due to Ca^{2+}-activated Cl^- channels encoded by *Ano1* (aka *Tmem16a*). Although the Ca^{2+} dependence of *Ano1* is well

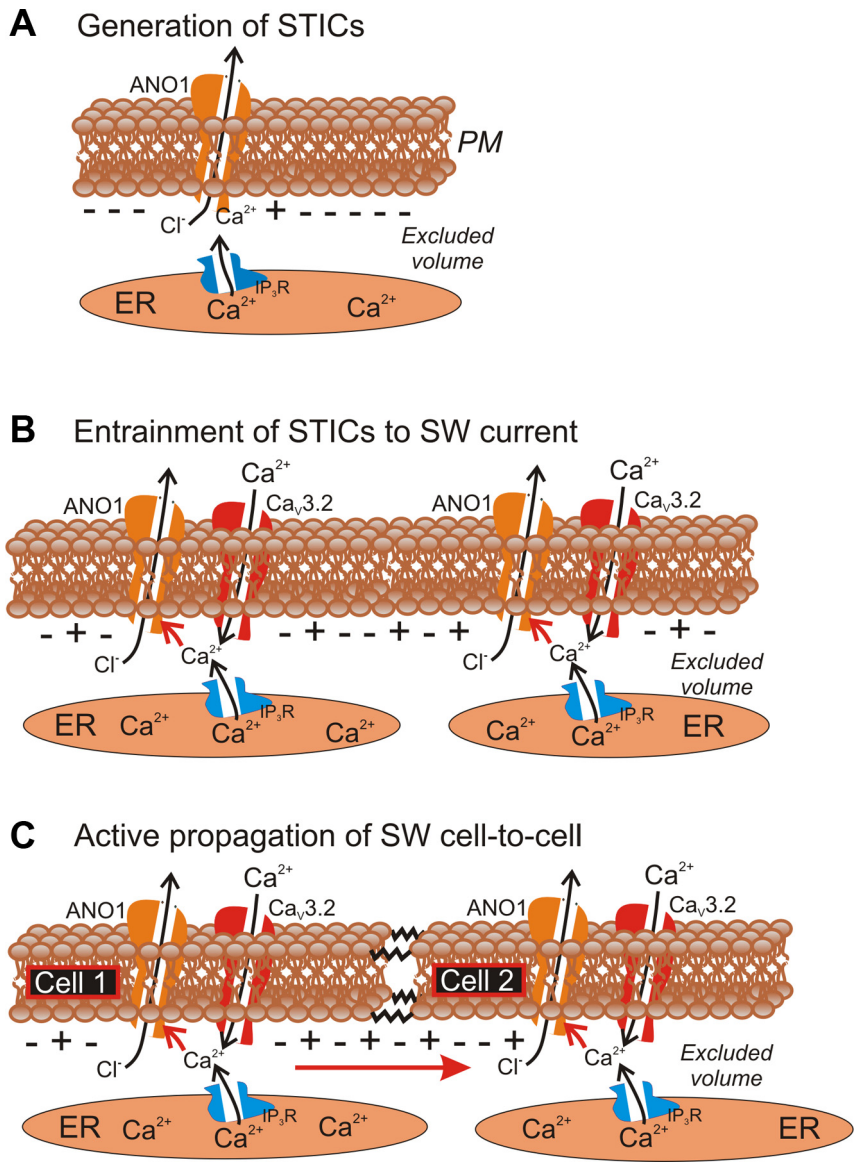

Fig. 9. Schematic showing role of T-current in pacemaker activity and propagation. *A*: localized Ca^{2+} release events in ICC activate nearby Ca^{2+}-activated Cl^- channels (Ano1) to create spontaneous transient inward currents (STICs). STICs produce spontaneous transient depolarizations of cell membrane. *B*: when a threshold potential is reached for regenerative activation of T-type channels ($Ca_V3.2$) Ca^{2+} entry reinforces activation of Ano1 and further depolarizes cell. This leads to generation of whole cell slow wave current. *C*: slow wave currents conduct (red arrow) to coupled cells (resistor symbols) and depolarize adjacent cells. Depolarization activates T-type currents in adjacent cells and Ca^{2+} entry and release in these cells activates Ano1 channels. This sequence explains cell-to-cell propagation of slow waves in ICC networks. IP_3, inositol triphosphate; ER, endoplasmic reticulum; SW, slow wave; PM, plasma membrane.

documented (2, 31, 38) and the requirement for Ca^{2+} entry for depolarization-dependent generation of slow wave currents was demonstrated (39), the mechanism for Ca^{2+} entry in native, freshly isolated ICC had not been described previously. ICC display a continuous discharge of STICs when held at negative potentials, and depolarization to about −65 mV elicits large amplitude slow wave currents. The voltage-dependent generation of slow wave currents is blocked by reduced $[Ca^{2+}]_o$, by replacing $[Ca^{2+}]_o$ with equimolar $[Ba^{2+}]_o$ and by Ni^{2+} (30 μM). These data suggest that entrainment of STICs into slow wave currents requires Ca^{2+} entry through the T-type conductance identified in the present study. We also envision a role for these channels in cell-to-cell propagation because depolarization caused by Ano1 slow wave currents will depolarize and activate T-type channels in coupled ICC. In the present study 30 μM Ni^{2+} decreased the frequency of slow waves and slowed upstroke velocities; however, this concentration of Ni^{2+} did not block pacemaker activity. As discussed above, propagation experiments are consistent with the involvement of a T-type conductance in propagation. Together with the data from the present study, pharmacological studies suggest that the following sequence of events in the generation and propagation of slow waves (Fig. 9): *1*) stochastic localized Ca^{2+} release events (puffs) are linked to local activation of clusters of Ca^{2+}-activated Cl^- channels, STICs; *2*) STICs cause variable amplitude transient depolarizations (STDs); *3*) STDs reach a threshold for regenerative activation of T-type Ca^{2+} channels; *4*) ensuing depolarization can also recruit L-type channels; *5*) Ca^{2+} entry through channels distributed through the cell membrane can elicit Ca^{2+}-induced Ca^{2+} release nearly simultaneously from Ca^{2+} stores (i.e., entraining Ca^{2+} release); *6*) simultaneous Ca^{2+} release, summing with Ca^{2+} entry, elicits whole cell slow wave currents; and *7*) these currents result in slow wave depolarization that conducts to coupled cells and evokes whole cell slow wave currents progressively cell-to-cell through the ICC network. Missing from the above scheme, at present, are direct measurements of Ca^{2+} puffs or entrainment of localized Ca^{2+} transients into multisite or whole cell Ca^{2+} transients in ICC in response to depolarization and Ca^{2+} entry via T-type Ca^{2+}. The small size of ICC and the need to locate these cells in mixed cell dispersions with a fluorescent reporter have made such measurements difficult to obtain.

ACKNOWLEDGMENTS

We are grateful to Lauren E. Peri for performing the PCR studies of Ca^{2+} channel gene expression, Jared B. Townsend for sorting cells by FACS, Nancy Horowitz for technical assistance, and Huili Zheng for help with breeding and maintenance of the transgenic animals. smMHC/Cre/eGFP mice were donated by Michael Kotlikoff, Cornell University, and *Cacna1h*$^{-/-}$ mice were provided by Kevin P Campbell, University of Iowa.

GRANTS

This work was supported by National Institute of Diabetes and Digestive and Kidney Diseases Grant P01-DK-41315.

DISCLOSURES

No conflicts of interest, financial or otherwise, are declared by the author(s).

AUTHOR CONTRIBUTIONS

Author contributions: H.Z., K.S.P., S.D.K., and K.M.S. conception and design of research; H.Z. and K.S.P. performed experiments; H.Z., K.S.P., and S.D.K. analyzed data; H.Z., S.D.K., and K.M.S. interpreted results of experiments; H.Z. and K.S.P. prepared figures; H.Z., S.D.K., and K.M.S. drafted manuscript; H.Z., S.D.K., and K.M.S. edited and revised manuscript; H.Z., K.S.P., S.D.K., and K.M.S. approved final version of manuscript.

REFERENCES

1. **Bayguinov O, Ward SM, Kenyon JL, Sanders KM.** Voltage-gated Ca^{2+} currents are necessary for slow-wave propagation in the canine gastric antrum. *Am J Physiol Cell Physiol* 293: C1645–C1659, 2007.
2. **Caputo A, Caci E, Ferrera L, Pedemonte N, Barsanti C, Sondo E, Pfeffer U, Ravazzolo R, Zegarra-Moran O, Galietta LJ.** TMEM16A, a membrane protein associated with calcium-dependent chloride channel activity. *Science* 322: 590–594, 2008.
3. **Catterall WA, Perez-Reyes E, Snutch TP, Striessnig J.** International Union of Pharmacology. XLVIII. Nomenclature and structure-function relationships of voltage-gated calcium channels. *Pharmacol Rev* 57: 411–425, 2005.
4. **Dickens EJ, Hirst GD, Tomita T.** Identification of rhythmically active cells in guinea-pig stomach. *J Physiol* 514: 515–531, 1999.
5. **Edwards FR, Hirst GD.** An electrical analysis of slow wave propagation in the guinea-pig gastric antrum. *J Physiol* 571: 179–189, 2006.
6. **Gibbons SJ, Strege PR, Lei S, Roeder JL, Mazzone A, Ou Y, Rich A, Farrugia G.** The alpha1H Ca^{2+} channel subunit is expressed in mouse jejunal interstitial cells of Cajal and myocytes. *J Cell Mol Med* 13: 4422–4431, 2009.
7. **Goto K, Matsuoka S, Noma A.** Two types of spontaneous depolarizations in the interstitial cells freshly prepared from the murine small intestine. *J Physiol* 559: 411–422, 2004.
8. **Hennig GW, Hirst GD, Park KJ, Smith CB, Sanders KM, Ward SM, Smith TK.** Propagation of pacemaker activity in the guinea-pig antrum. *J Physiol* 556: 585–599, 2004.
9. **Hirst GD, Bramich NJ, Teramoto N, Suzuki H, Edwards FR.** Regenerative component of slow waves in the guinea-pig gastric antrum involves a delayed increase in $[Ca^{2+}]_i$ and Cl^- channels. *J Physiol* 540: 907–919, 2002.
10. **Hirst GD, Edwards FR.** Generation of slow waves in the antral region of guinea-pig stomach–a stochastic process. *J Physiol* 535: 165–180, 2001.
11. **Huizinga JD, Thuneberg L, Kluppel M, Malysz J, Mikkelsen HB, Bernstein A.** W/kit gene required for interstitial cells of Cajal and for intestinal pacemaker activity. *Nature* 373: 347–349, 1995.
12. **Hwang SJ, Blair PJ, Britton FC, O'Driscoll KE, Hennig G, Bayguinov YR, Rock JR, Harfe BD, Sanders KM, Ward SM.** Expression of anoctamin 1/TMEM16A by interstitial cells of Cajal is fundamental for slow wave activity in gastrointestinal muscles. *J Physiol* 587: 4887–4904, 2009.
13. **Iftinca M, McKay BE, Snutch TP, McRory JE, Turner RW, Zamponi GW.** Temperature dependence of T-type calcium channel gating. *Neuroscience* 142: 1031–1042, 2006.
14. **Imtiaz MS, Katnik CP, Smith DW, van Helden DF.** Role of voltage-dependent modulation of store Ca^{2+} release in synchronization of Ca^{2+} oscillations. *Biophys J* 90: 1–23, 2006.
15. **Kim YC, Koh SD, Sanders KM.** Voltage-dependent inward currents of interstitial cells of Cajal from murine colon and small intestine. *J Physiol* 541: 797–810, 2002.
16. **Kito Y, Suzuki H.** Effects of temperature on pacemaker potentials in the mouse small intestine. *Pflügers Arch* 454: 263–275, 2007.
17. **Kito Y, Suzuki H.** Properties of pacemaker potentials recorded from myenteric interstitial cells of Cajal distributed in the mouse small intestine. *J Physiol* 553: 803–818, 2003.
18. **Kito Y, Ward SM, Sanders KM.** Pacemaker potentials generated by interstitial cells of Cajal in the murine intestine. *Am J Physiol Cell Physiol* 288: C710–C720, 2005.
19. **Langton P, Ward SM, Carl A, Norell MA, Sanders KM.** Spontaneous electrical activity of interstitial cells of Cajal isolated from canine proximal colon. *Proc Natl Acad Sci USA* 86: 7280–7284, 1989.
20. **Mak DO, McBride S, Foskett JK.** Inositol 1,4,5-trisphosphate [correction of tris-phosphate] activation of inositol tris-phosphate receptor Ca^{2+} channel by ligand tuning of Ca^{2+} inhibition. *Proc Natl Acad Sci USA* 95: 15821–15825, 1998.
21. **Malysz J, Donnelly G, Huizinga JD.** Regulation of slow wave frequency by IP_3-sensitive calcium release in the murine small intestine. *Am J Physiol Gastrointest Liver Physiol* 280: G439–G448, 2001.

22. **Mason MJ, Mahaut-Smith MP.** Voltage-dependent Ca^{2+} release in rat megakaryocytes requires functional IP3 receptors. *J Physiol* 533: 175–183, 2001.
23. **Nakamura E, Kito Y, Hashitani H, Suzuki H.** Metabolic component of the temperature-sensitivity of slow waves recorded from gastric muscle of the guinea-pig. *J Smooth Muscle Res* 42: 33–48, 2006.
24. **Nose K, Suzuki H, Kannan H.** Voltage dependency of the frequency of slow waves in antrum smooth muscle of the guinea-pig stomach. *Jpn J Physiol* 50: 625–633, 2000.
25. **Ordog T, Ward SM, Sanders KM.** Interstitial cells of Cajal generate electrical slow waves in the murine stomach. *J Physiol* 518: 257–269, 1999.
26. **Ozaki H, Stevens RJ, Blondfield DP, Publicover NG, Sanders KM.** Simultaneous measurement of membrane potential, cytosolic Ca^{2+}, and tension in intact smooth muscles. *Am J Physiol Cell Physiol* 260: C917–C925, 1991.
27. **Park KJ, Hennig GW, Lee HT, Spencer NJ, Ward SM, Smith TK, Sanders KM.** Spatial and temporal mapping of pacemaker activity in interstitial cells of Cajal in mouse ileum in situ. *Am J Physiol Cell Physiol* 290: C1411–C1427, 2006.
28. **Sanders KM.** A case for interstitial cells of Cajal as pacemakers and mediators of neurotransmission in the gastrointestinal tract. *Gastroenterology* 111: 492–515, 1996.
29. **Sanders KM.** Ionic mechanisms of electrical rhythmicity in gastrointestinal smooth muscles. *Annu Rev Physiol* 54: 439–453, 1992.
30. **Sanders KM, Koh SD, Ward SM.** Interstitial cells of cajal as pacemakers in the gastrointestinal tract. *Annu Rev Physiol* 68: 307–343, 2006.
31. **Schroeder BC, Cheng T, Jan YN, Jan LY.** Expression cloning of TMEM16A as a calcium-activated chloride channel subunit. *Cell* 134: 1019–1029, 2008.
32. **Tomita T.** Electrical activity (spikes and slow waves) in gastrointestinal smooth muscle. In: *Smooth Muscle, An Assessment of Current Knowledge*. Austin, TX: Univ. of Texas Press, 1981, p. 127–156.
33. **Torihashi S, Ward SM, Nishikawa S, Nishi K, Kobayashi S, Sanders KM.** c-kit-dependent development of interstitial cells and electrical activity in the murine gastrointestinal tract. *Cell Tissue Res* 280: 97–111, 1995.
34. **van Helden DF, Imtiaz MS.** Ca^{2+} phase waves: a basis for cellular pacemaking and long-range synchronicity in the guinea-pig gastric pylorus. *J Physiol* 548: 271–296, 2003.
35. **Ward SM, Baker SA, de Faoite A, Sanders KM.** Propagation of slow waves requires IP3 receptors and mitochondrial Ca^{2+} uptake in canine colonic muscles. *J Physiol* 549: 207–218, 2003.
36. **Ward SM, Burns AJ, Torihashi S, Sanders KM.** Mutation of the proto-oncogene c-kit blocks development of interstitial cells and electrical rhythmicity in murine intestine. *J Physiol* 480: 91–97, 1994.
37. **Ward SM, Vogalis F, Blondfield DP, Ozaki H, Fusetani N, Uemura D, Publicover NG, Sanders KM.** Inhibition of electrical slow waves and Ca^{2+} currents of gastric and colonic smooth muscle by phosphatase inhibitors. *Am J Physiol Cell Physiol* 261: C64–C70, 1991.
38. **Yang YD, Cho H, Koo JY, Tak MH, Cho Y, Shim WS, Park SP, Lee J, Lee B, Kim BM, Raouf R, Shin YK, Oh U.** TMEM16A confers receptor-activated calcium-dependent chloride conductance. *Nature* 455: 1210–1215, 2008.
39. **Zhu MH, Kim TW, Ro S, Yan W, Ward SM, Koh SD, Sanders KM.** A Ca^{2+}-activated Cl^- conductance in interstitial cells of Cajal linked to slow wave currents and pacemaker activity. *J Physiol* 587: 4905–4918, 2009.
40. **Zhu MH, Sung IK, Zheng H, Sung TS, Britton FC, O'Driscoll K, Koh SD, Sanders KM.** Muscarinic activation of Ca^{2+}-activated Cl^- current in interstitial cells of Cajal. *J Physiol* 589: 4565–4582, 2011.